ELSEVIER

Thermochimica Acta 243 (1994) 115–127

thermochimica acta

A new high-performance thermoplastic polyimide and its fiber-reinforced composites ☆

Bryan P. Livengood, Tammy M. Chalmers, Yi Gu, Yi-Ding Zhang, Frank W. Harris, Stephen Z.D. Cheng *

Maurice Morton Institute and Department of Polymer Science, The University of Akron, Akron, OH 44325-3909, USA

Received 4 February 1994; accepted 14 April 1994

Abstract

A new high-performance thermoplastic polyimide has recently been synthesized from 3,3′,4,4′-benzophenonecarboxylic dianhydride (BTDA) and 2,2′-dimethyl-1,3-(4-aminophenoxy)propane (DMDA). It has been shown to possess good dimensional and thermal stability, as well as exhibiting excellent mechanical properties, in particular the extraordinary toughness of BTDA–DMDA with a fracture energy G_{1C} value of 4.28 kJ m^{-2}, which exceeds that of other high-performance materials by about 100%. Clearly, this material has great potential as a matrix resin for high-temperature, high-performance composites. This report focuses on the study of this polymer's structure, crystal morphology, crystal–amorphous interface and relaxation processes in order to find the origin of this unusually high toughness. In addition to this, we have also examined the matrix/fiber interfaces of BTDA–DMDA-based carbon fiber and polyimide fiber-reinforced composites via their mechanical properties, and then their crystallization and relaxation behaviors.

Keywords: BTDA–DMDA; Composite; Polyimide; Stability; Thermoplastic; Toughness

1. Introduction

Aromatic polyimides, as a class of polymeric materials, show excellent mechanical properties with high thermal and thermo-oxidative stability, good chemical and

☆ Presented at the 22nd Annual NATAS Conference, Denver, CO, 19–22 September 1993.

* Corresponding author.

SSDI 0040-6031(94)01819-3

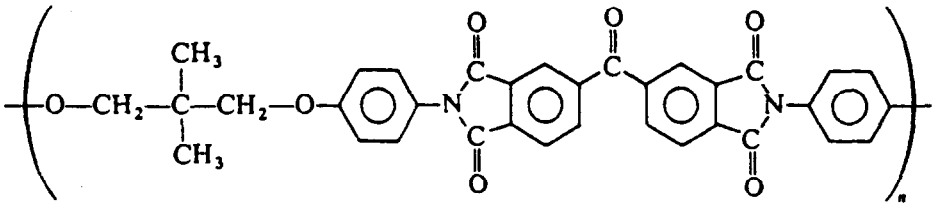

Structure 1. BTDA–DMDA.

light resistance, and low dielectric constants. The combination of these superior properties leads to a wide use of polyimides in many different applications such as coatings, films and matrix resins in structural composites. Due to the necessity of developing new impact/solvent resistant composite resins for structural materials in aerospace applications, a new polyimide has been synthesized from 3,3′,4,4′-benzophenonecarboxylic dianhydride (BTDA) and 2,2′-dimethyl-1,3-(4-aminophenoxy)propane (DMDA) at the University of Akron [1]. The chemical structure of this new polymer (BTDA–DMDA) is shown in Structure 1, and the molecular weight of its repeat unit is 572 g mol^{-1}. The thermal and thermo-oxidative stabilities have been studied, and this polyimide's activation energies for decomposition obtained by thermogravimetry (TGA) in air and nitrogen are about 150 and 154 kJ mol^{-1}, respectively [2], very close to that of poly(*p*-phenylene sulfide) (PPS). BTDA–DMDA is a semicrystalline polyimide with a glass transition temperature of 230°C and a heat capacity increase of 145 J K^{-1} mol^{-1} at the T_g. Also, its apparent melting point is around 320°C. Fig. 1 shows the heat capacity data of a

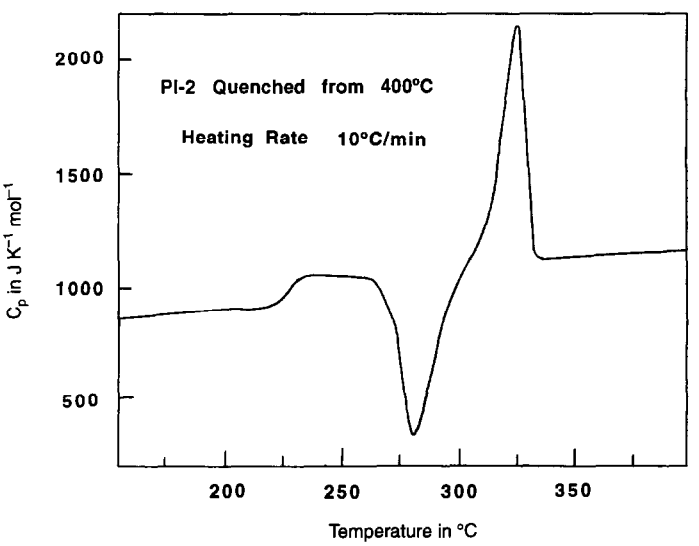

Fig. 1. A heat capacity curve of a BTDA–BMDA sample quenched from the melt before the measurement.

Table 1
Neat resin properties of BTDA–DMDA

Property	Average value	Test method
Fracture energy/(kJ m^{-2})	4.28	Double torsion
Flexural modulus/(GPa)	3.00	ASTM D790M-86
Shear modulus/(GPa)	1.54	Calculated from tensile modulus and Poisson ratio
Tensile strength/(MPa)	95.2	ASTM D638M-89
Tensile modulus/(GPa)	4.05	ASTM D638M-89
Poisson ratio	0.32	ASTM E132-86

BTDA–DMDA sample quenched from the melt to liquid nitrogen before the measurement. This leads to a crystallization window of only 90°C, compared to that seen for PEEK at 190°C and PPS of 180°C [1]. From its oriented wide-angle X-ray diffraction fiber pattern, the crystal structure was determined to be monoclinic with dimensions of $a = 0.960$ nm, $b = 0.582$ nm, $c = 2.46$ nm and $\gamma = 81.1°$ [1]. The crystal morphology has been observed via polarized light and transmission electron microscopes (PLM and TEM). No mature spherulites can be found [1]. The degree of crystallinity has been found to be around 20–30% in melt processing, and can reach 50% by solution-induced crystallization [1]. The mechanical properties of this polyimide are listed in Table 1. A particulary important property is the fracture energy G_{1C}, which reaches 4.28 kJ m^{-2} [3]. This value is about 100% higher than the commercially available thermoplastic engineering polymers such as poly(aryl ether ether ketone)s (PEEKs) and PPS.

In this paper, we focus on two objectives of this ongoing research: to identify the contributing factors of the extraordinary high toughness of this polymer, and to examine the property differences of the two different types of fiber-reinforced composites. The type of fibers used in the first were carbon fibers without surface treatment, and therefore, the fiber surface is non-polar. The second type of fibers studied were aromatic polyimide fibers spun in our laboratory [4–6], with the fiber surfaces being polar. The aromatic polyimide was synthesized from 3,3′,4,4′-tetracarboxy-biphenyl dianhydride (BPDA) and 2,2′-dimethyl-4,4′-diaminobiphenyl (DMB) for the fiber spinning. To determine the results, we have examined the thermal behavior differences of the interfacial regions of the resins and fibers in these composites.

2. Experimental

2.1. Materials

BTDA–DMDA was synthesized from 3,3′,4,4′-benzophenonecarboxylic dianhydride (BTDA) and 2,2′-dimethyl-1,3-(4-aminophenoxy)propane (DMDA). A detailed procedure for the synthesis has been reported previously [1]. The resin was

obtained as a poly(amic acid) solution in THF/NMP. The T650 carbon fiber was acquired from Amoco and used without any additional modification. Finally, the BPDA–DMB polyimide fibers were also synthesized and spun in our laboratories [4–6].

2.2. Composite fabrication

The carbon fibers were first coated with matrix material and then wound onto a drum coated with teflon release tape. The solvent was then allowed to evaporate at room temperature for several hours. Twenty-two plies were then stacked together in a compression mold, which was then heated at 2°C min^{-1} to 300°C while 27 MPa of pressure was applied. The mold was held at this temperature for one hour and finally air-cooled to room temperature. C-scans were performed on the finished parts to guarantee the absence of voids. The polyimide fibers were wound by hand around metal blocks, which were then coated with the BTDA–DMDA matrix material. The prepegs were heated to 250°C in a vacuum oven to remove solvent and then imidized at 250°C for 2 h. Forty plies were stacked together in a compression mold and the same procedure as described above was used to mold the samples. Composite samples, carbon-fiber- as well as polyimide-fiber-reinforced, were analyzed as prepeg parts which contained 40 wt% BTDA–DMDA matrix resin.

2.3. Characterization experiments

Isothermal crystallization experiments were completed on a Du Pont 910 DSC for the BTDA–DMDA resin and its carbon-fiber-reinforced composite and on a Seiko 220 DSC for the polyimide-fiber-reinforced composite. Both the resin and composite samples were heated to 360°C on a hot stage and held there for two minutes in order to ensure complete melting. The samples were then quenched to a preset crystallization temperature (240–310°C) as rapidly as experimentally feasible. After crystallization was complete, the samples were re-heated without prior cooling at 10°C min^{-1} to 400°C. Each specimen was subsequently used only once. Thermal transition behavior was also examined using a Perkin-Elmer DSC2 coupled with an IBM computer. The temperature and heat flow scales for the three DSCs were calibrated with standard melting materials over a temperature range of 25–400°C. All experiments were completed in a dry nitrogen atmosphere and the heating rate was 10°C min^{-1}.

Wide-angle X-ray diffraction (WAXD) experiments were conducted on a Rigaku 12 kW rotating anode as the source of the incident X-ray beam. These tests were carried out on both the neat resin and the carbon fiber composite samples, which were then given thermal treatments paralleling those for the DSC experiments. For all specimens, the crystallinity was determined using Ruland's method over a diffraction angle (2θ) of 5°–80°. Also, the apparent crystallite sizes were determined to a first approximation using Scherrer's equation.

Polarized light microscopy (PLM) experiments were performed on an Olympus BH-2 microscope coupled with a Linkam TMS91 hot stage. Samples were heat-treated as described above for the DSC experiments and prepared on microscopy glass slides. The sample thickness was 10 μm.

Scanning electron microscopy (SEM) studies were carried out on the BTDA–DMDA neat resin, as well as on the T650 carbon-fiber- and polyimide-fiber-reinforced composites. The specimens were prepared by freeze fracturing them while submersed in liguid nitrogen. After fracture the samples were subjected to an *o*-phosphoric acid etching. The specimens were then sputter-coated with Au/Pd (60:40) and studied with a JEOL/JSM U3 SEM with 25 kV accelerating voltage.

Dynamic mechanical thermal analysis (DMA) experiments were performed using a Du Pont 983 DMA coupled with a TA Instruments 2000 Thermal Analyzer. Relaxations were examined by scanning the samples from -150 to 400°C at 5°C min^{-1} in a dry nitrogen atmosphere. The DMA instrument was operated in its fixed frequency mode from 0.1 to 10 Hz.

3. Results and discussion

3.1. The contributing factors to BTDA–DMDA's high toughness

We have discovered that there are three structure and morphology levels of different sizes in the BTDA–DMDA resin, which all contribute to this material's extraordinary toughness: (1) sub-glass (secondary) relaxation processes caused by BTDA–DMDA's chemical structure design, (2) unusual crystal morphology, and (3) the crystalline–amorphous interfacial structures. Combining these three effects without a doubt justifies the high fracture toughness obtained.

The relaxation behavior of BTDA–DMDA resin and its carbon fiber composite have been examined. Fig. 2 shows typical storage modulus (E') and loss factor (E'') plots at different frequencies and temperatures for the neat resin. Three distinct relaxations can clearly be recognized. The highest temperature relaxation, commonly called the α-relaxation, refers to the glass transition and is located in the 230–250°C range, depending on annealing conditions and observation frequency. The middle transition peak, also known as the β-relaxation, occurs at approximately 100°C. Finally, the lowest temperature relaxation peak of the γ-relaxation exists at roughly -100°C. It can be hypothesized from these results that the two secondary relaxations provide a broad spectrum through which energy may be dissipated, thus increasing the toughness of this material. DMA measurements from different frequencies have been used to calculate the activation energies of these three transitions based on the Arrhenius equation. These results are shown in Fig. 3, again for the BTDA–DMDA neat resin. From the plots, the γ-relaxation clearly possesses the lowest activation energy at 44 kJ mol^{-1}, followed by the β-relaxation with a value of 182 kJ mol^{-1}. Finally, the α-relaxation, with a value of 420 kJ mol^{-1}, has the highest activation energy of the three transitions. Note that, in principle, a single relaxation process described by the Arrhenius equation does not

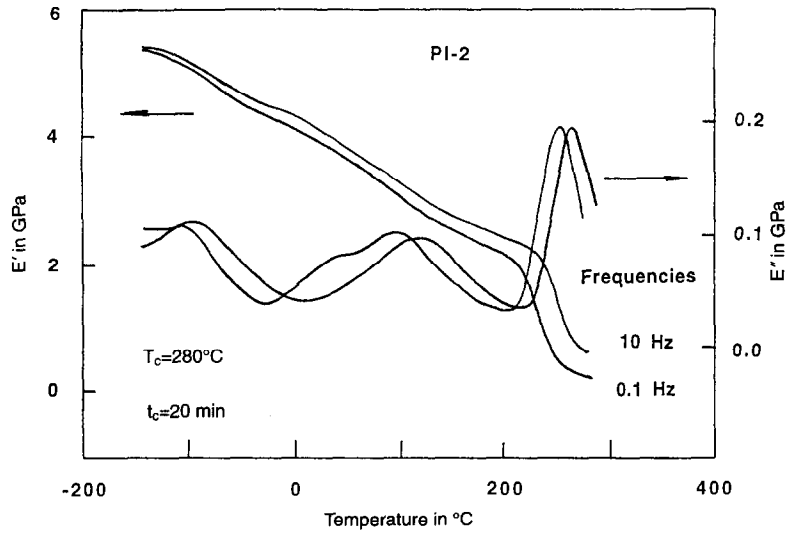

Fig. 2. A DMA diagram of E' and E'' for the semi-crystalline BTDA–DMDA sample.

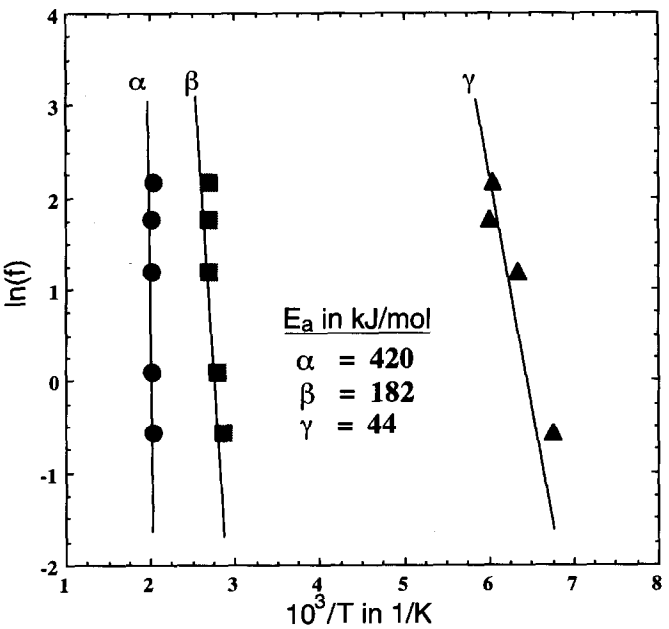

Fig. 3. A plot of logarithmic frequency and reciprocal peak temperature of the loss factors for BTDA–DMDA.

describe a glass transition process. Instead, a WLF equation should be used for this transition with multi-relaxation processes. As a result, the plot in Fig. 3 for the α-relaxation should not be linear, but curved. However, because the frequency

range in DMA is only three to four order of magnitudes, it is not broad enough for the observation of this curvature. The plot shown in Fig. 3 thus represents an apparent activation energy. In order to extend to high frequencies, dielectric analysis must be used. Furthermore, ^{13}C solid-state NMR experiments are currently being utilized to investigate the molecular motions corresponding to these three relaxation processes.

In addition to the DMA results, DSC and WAXD observaions also support a mechanism for increased toughness in proving the existence of a rigid-amorphous fraction in the BTDA–DMDA sample. The concept of a "rigid-amorphous fraction" has been investigated previously above the glass transition temperature for a few thermoplastic engineering polymers [7–9]. This study involved detailed thermal analysis experiments in both the glass transition and crystal melting regions. It is well-known that the heat capacity increase at glass transition is due to the molecular motions of the amorphous fraction region in a semicrystalline sample, while the crystal melting is attributed to the fusion of the crystalline fraction region. If the classical crystallinity (two-phase) model holds, the summation of these two fractions should be equal to one. Nevertheless, in many semicrystalline polymers, the summation is always less than one, indicating that there is a fraction which is still rigid above the glass transition. Therefore, it does not contribute to the heat capacity increase at T_g, but gradually relaxes at higher temperatures. However, this fraction of material is not crystalline, and does not take part in the crystal melting. For BTDA–BMDA resins, it was further found in these experiments that with increasing amounts of crystallinity in this polymer, the amount of rigid-amorphous fraction also increases, while the apparent crystallite sizes remain constant with crystallization temperature and time. This leads to the conclusion that the amount of rigid-amorphous fraction is proportional to the crystal surface area, and consequently, to the amount of interface between the crystalline and amorphous regions [2]. Moreover, as much as 50% of the BTDA–DMDA can be included in this fraction. Therefore, it can be understood that this interfacial region or rigid-amorphous fraction is also a contributing factor to the high toughness of this matrix material.

Another interesting phenomenon was observed in exploring the crystal morphology of BTDA–DMDA. No mature spherulites were seen when this neat resin was examined under polarized light microscopy (PLM). Also, in analyzing the sample under the transmission electron microscope (TEM), it was found that only randomly stacked lamellar crystals were observed displaying a lateral size of less than 3 mm. The long spacing of these lamellar crystals has been calculated to be approximately 10–20 nm for this polymer [1]. It is extremely important to note that this characteristic and beneficial morphology does not change with different crystallization conditions, as a result of this material's narrow crystallization window ($T_m - T_g = 90°C$). As a consequence, although microcracks may form as they usually do in other thermoplastic engineering polymers, the absence of mature spherulites does not provide a weak path for microcrack propagation along spherulite boundaries. These cracks are stopped when the propagation meets a lamellar crystal. Therefore, this kind of crystal morphology also increases the toughness of the BTDA–BMDA resin.

3.2. Interfacial properties between matrix and fibers

The fracture energy G_{1C} was measured for the (BTDA–DMDA)/T650 carbon fiber composites. The value decreased from 4.28 kJ m^{-2} for the neat resin to 1.81 kJ m^{-2} for the composite when measured via the double cantilever beam method. Even though there is a fiber effect which constrains the matrix material in the composite along the fiber direction, it is believed that this dramatic decrease in toughness mainly results from the weak interface between the carbon fibers and the matrix. This is due to the surface of the carbon fibers being non-polar. Thus, a probable method of alleviating this problem would be to use fibers similar in polarity and chemical structure to the BTDA–DMDA material, therefore increasing the favorable interactions at the interface. This is why polyimide fibers were then chosen to be studied for the BTDA–DMDA-based fiber-reinforced composites. Some of the results for this type of system are shown below and others are currently being investigated.

It has been found that the phase transition and isothermal crystallization kinetics behavior of the (BTDA–DMDA)/T650 carbon fiber composites show no deviation from those previously reported for the neat resin as listed in Table 2. Thus, as expected, these conclusions support our prediction of a limited or non-existent interface between the carbon fibers and the polyimide matrix material, which at least partially contributes to the large decrease in fracture energy. In addition to these results, it was found that the presence of carbon fibers does not change the degree of crystallinity obtained for these samples, nor does it affect the apparent crystallite sizes, as seen in the WAXD experiments. The results are listed in Table 3. Furthermore, the relaxation behavior studied via DMA does not change from what was seen in the neat resin. For example, the activation energies of the β-relaxation for the BTDA–DMDA in the resin and in the carbon fiber composite are 182 and 180 kJ mol^{-1}, respectively. The effect of the T650 carbon fibers on the crystallization processes of the BTDA–DMDA matrix in the fiber-reinforced composites has also been studied through polarized light microscopy (PLM). As

Table 2
The peak crystallization time for neat resin and carbon-fiber-based composites

Crystallization temperature in °C	Crystallization [a] peak time in min	Crystallization [b] peak time in min
240	1.6	1.5
250	1.2	1.3
260	1.0	0.98
270	0.92	0.93
280	0.85	0.87
290	0.90	0.91
300	1.0	1.1

[a] Crystallization peak time of the BTDA–DMDA resin. [b] Crystallization peak time of the carbon fiber–(BTDA–DMDA) composite.

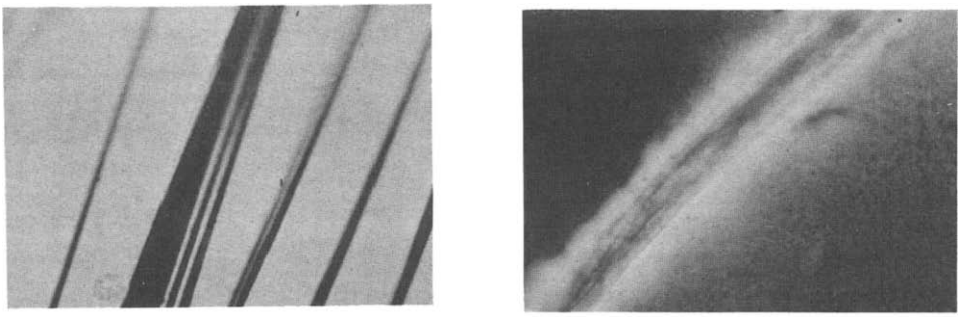

(a) (b)

Fig. 4. PLM photographs of crystal morphology for carbon (a) and polyimide (b) fibers in the BTDA–DMDA matrix.

Table 3
Crystallinities and apparent crystallite sizes for BTDA–DMDA resins and (BTDA–DMDA)/T650 composites

Crystallization temperature in °C	Resins		Composites	
	w^c in % [a]	(200) size [b] in nm	w^c in % [a]	(200) size [b] in nm
260	29	88	27	85
270	27	90	25	86
280	27	85	26	86
290	28	89	25	88
300	28	88	27	87

[a] The crystallinities were measured via DSC. [b] The (200) apparent crystallite sizes were measured via WAXD experiments.

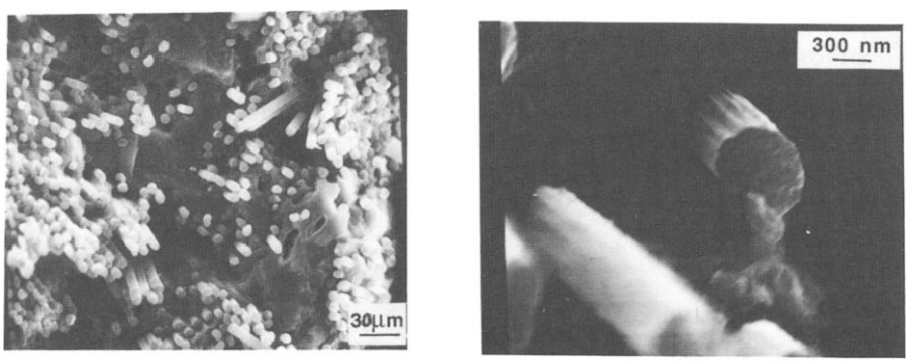

(a) (b)

Fig. 5. SEM photographs for the fracture surface of a (BTDA–DMDA)/carbon fiber composite.

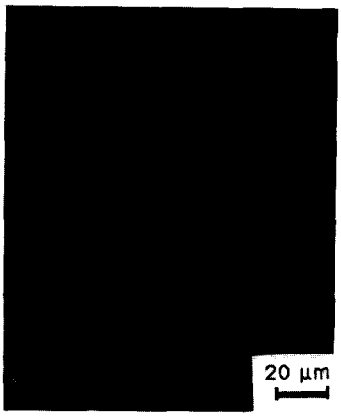

Fig. 6. SEM photograph for the fracture surface of a (BTDA–DMDA)/polyimide fiber composite.

shown in Fig. 4, it is apparent that there is no observable transcrystallization [10] occurring on the carbon fiber surface. On a smaller microscopic level, SEM investigations also provided conclusive evidence for the lack of beneficial matrix/fiber interactions as can be seen in Fig. 5. The fracture surface of these carbon fiber composites mainly shows fiber pull-out as the mechanism of failure.

BTDA–BMDA matrix/polyimide fiber composites were studied in an effort to solve the problem of poor matrix/fiber interfacial adhesion. As seen in Fig. 4 through PLM, a transcrystallization process [10] has definitely occurred, in contrast to the unfavorable results obtained for the T650 carbon-fiber-based composites. These polyimide-fiber-based composites have also been examined with a scanning electron microscope. Fig. 6 shows that BTDA–DMDA matrix material has adhered to the fibers after the samples were freeze-fractured. This indicates that the mechanism of failure is not entirely fiber pull out, but is somewhat cohesive in nature. One of the major factors that enhances the matrix/fiber interface in the polyimide fiber-reinforced composites is the compatibility of the two components in reference to their polarity. In the (BTDA–DMDA)/carbon fiber composites, the interface is non-polar/polar and the system exhibits poor interfacial adhesion, while the interface between the (BTDA–DMDA)/polyimide fiber composites possesses a polar–polar interaction. Therefore, from these results we can conclude that the polyimide fiber composites will have much higher fracture energy values compared to the carbon fiber composites, and hopefully this value will approach that of the BTDA–DMDA neat resin. This would prove to be a major advance in the area of polyimide-based composites, because of the fact that the toughness of these systems is one of the main limiting factors in their lack of use as high-performance composite materials.

The isothermal crystallization behavior of these composites has also been investigated. The results from these experiments suggest that the crystallization process is a two-step process, in contrast to that of the BTDA–BMDA neat resin which is just a one-step crystallization process. This was deduced from the results of the

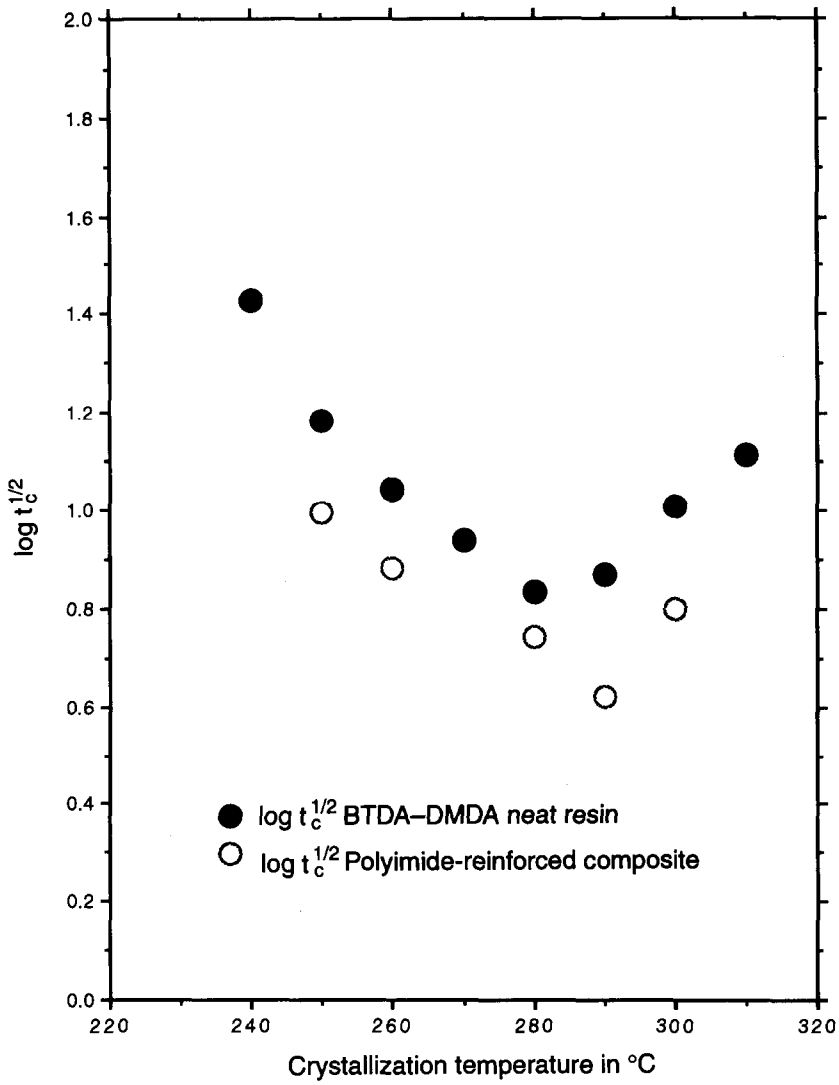

Fig. 7. A plot of peak crystallization time versus crystallization temperature for both BTDA–DMDA resin and (BTDA–DMDA)/polyimide fiber composites.

Avrami kinetics plots for various crystallization temperatures. There is a distinct change in the value of n, the slope of the Avrami plot (Avrami exponent), from 3 to 2 in the early crystallization process at around 8%–10% crystallinity. Note that for the BTDA-DMDA resin, the Avrami exponent of approximately 2 for all examined isothermal crystallization temperatures reveals a ribbon type of lamellar crystal growth based on the TEM morphological observations [1]. In the composite case, the fact that the Avrami exponent is 3 initially might be an indication of a combined growth of both fiber-surface-induced transcrystallization and ribbon

lamellar crystal growth. Furthermore, the transcrystallization occurs at the fiber surface where the fibers act as nucleation sites, and this kind of crystallization is most likely one-dimensional ($n = 1$) [11]. The crystallization peak time can also be used as a measure of the crystallization rate. In Fig. 7, the crystallization peak time versus the crystallization temperature data has been plotted for both the polyimide fiber composites and the neat resin. The polyimide fibers clearly affect the crystallization kinetics of the BTDA–DMDA as seen in the substantial decrease in the crystallization peak time (faster crystallization). We expect that these types of (BTDA–DMDA)/polyimide fiber composites possess a higher fracture toughness compared to that in the carbon-fiber-based composites. A further study and fabrication of the polyimide fiber-reinforced composites is an ongoing research topic in our laboratory.

4. Conclusions

Three different size levels in structure and crystal morphology: (1) the existence of the crystal–amorphous interface; (2) the observations of only randomly stacked ribbon-like lamellae and no mature spherulites; and (3) the detection of two sub-glass relaxation processes have been invoked in BTDA–DMDA, a thermoplastic polyimide neat resin, in the hope of explaining the unusually high toughness found in this material. Also, this polymer's surface-untreated T650 carbon fiber composite was studied and showed little or no matrix/fiber interactions (adhesion), which in particular causes the toughness of this system to be much lower than that of the neat resin, due to the mechanism of failure being adhesive rather than cohesive in nature. A polyimide-fiber-based composite for this matrix has also been examined. Contrary to the previous results, this system does show partial cohesive failure at the (BTDA–DMDA)/fiber interface rather than complete adhesive failure or fiber pull-out. A transcrystallization process, as expected between the two chemically similar polar components occurs which increases the interfacial strength between the matrix and the fiber surface. Therefore, it is assumed that the toughness of this type of composite will be much greater than that of the carbon fiber/(BTDA–DMDA) composites.

Acknowledgement

This work was supported by SZDC's Presidential Young Investigator Award (DMR-9175538) from the National Science Foundation and Center for Molecular and Microstructure Composites established by NSF/Ohio/EPIC.

References

[1] S.Z.D. Cheng, M.L. Mittleman, J.J. Janimak, D. Shen, T.M. Chalmers, S.H.-S. Lien, C.C. Tso, P.A. Gabori and F.W. Harris, Polym. Int. 29 (1992) 201.

[2] T.M. Chalmers, A. Zhang, D. Shen, S.H.-S. Lien, C.C. Tso, P.A. Gabori, F.W. Harris and S.Z.D. Cheng, Polym. Int. 31 (1993) 261.
[3] F.W. Harris, S.H.-S. Lien, P.A. Gabori, Y. Zhang, T.M. Chalmers, A. Zhang, D. Shen and Cheng, S.Z.D. Composite Structure, 27 (1994) 17.
[4] S.Z.D. Cheng, Z. Wu, A. Zhang, M. Eashoo, S.L.-C. Hsu and F.W. Harris, Polymer, 32 (1991) 1803.
[5] M. Eashoo, Z. Wu, D. Shen, A. Zhang, F.W. Harris, S.Z.D. Cheng, Polymer, 34 (1993) 3209.
[6] M. Eashoo, D. Shen, Z. Wu, F.W. Harris and S.Z.D. Cheng, Makromol. Chem., 195 (1994) 2207.
[7] S.Z.D. Cheng and B. Wunderlich, Macromolecules, 19 (1986) 1868; 20 (1987) 1630, 2082, 21, (1988) 789.
[8] S.Z.D. Cheng, D.P. Heberer, S.H.-S. Lien and F.W. Harris, J. Polym. Sci. Polym. Phys. Ed. 28 (1990) 655.
[9] S.Z.D. Cheng, J. Appl. Polym. Sci. Appl. Polym. Sci. Symp., 43 (1989) 315.
[10] B. Wunderlich, Macromolecular Physics, Crystal Structure, Morphology and Defect, Vol. 1, Academic Press, New York, 1972.
[11] B. Wunderlich, Macromolecular Physics, Crystal Nucleation, Growth, Annealing, Vol. 2, Academic Press, New York, 1976.